Low-Profile Low-Cost High Gain 60 GHz Antenna

YAZAN AL-ALEM[ID], **(Student Member, IEEE), AND AHMED A. KISHK, (Fellow, IEEE)**

Concordia University, Montréal, QC H3G 1M8, Canada

Corresponding author: Yazan Al-Alem (y_alalem@encs.concordia.ca)

ABSTRACT A new design perspective that utilizes the diffracted fields from planar metallic sheets to implement high gain, low profile, and low-cost antenna at 60 GHz is presented. The proposed antenna is matched over the 60-GHz ISM band (57–64 GHz). The proposed antenna can be employed in a linear antenna array with one wavelength distance between the array elements without generating grating lobes. The proposed antenna structure is suitable for short range, low power applications. The proposed antenna is vialess planar structure. The simplicity of the structure is advantageous in relaxing the fabrication process requirements.

INDEX TERMS Low profile antennas, millimeter-wave antenna, planar antenna, high gain antenna.

I. INTRODUCTION

The last decade has witnessed a high demand for high gain antennas at millimeter-wave frequencies. High gain antennas play an essential role in compensating the high path loss that wireless signals encounter at such frequencies [1], [2]. In the literature, various methods were employed to design high gain antennas at millimeter wave frequencies. In [3], an active microstrip antenna integrated with a three-stage pseudomorphic high electron mobility transistor amplifier was designed. Such an active antenna design is suitable for narrowband wireless local and personal area networks (WLAN/WPAN) applications. However, it demands a considerable amount of power consumption, which can constitute some limitations for mobile devices. In [4], a high gain array was comprised of radiating slots that are fed through the substrate integrated waveguide (SIW) power divider network. Such design is very robust in terms of its radiation characteristics because of the SIW feeding network, which is sufficiently shielded/packaged type of feeding networks [5]. On the other hand, it is comparatively expensive due to the required vias as compared with vialess planar structures. In [6], a 60 GHz antenna array with a dual-resonant slot-patch antenna was designed using LTCC technology. The shrinking effect of the LTCC substrates makes it more challenging and expensive in terms of its fabrication process. In [7], a monolithic polymer-based high gain Dielectric Resonator Antenna (DRA) was implemented efficiently. Nevertheless, such design would still require special fabrication process.

Adapting to the current requirements for the future generations of wireless technologies at millimeter wave frequencies, our present design focuses on the design of low cost, low profile, planar, and high gain antenna at 60 GHz. The structure suits short range, low power applications, such as wireless personal area networks (WPAN). The structure avoids using vias and any complex fabrication requirements, to be realized in any modest fabrication facility. The antenna utilizes the diffracted fields from plane metallic sheets to achieve a gain of 11 dBi. The antenna has a matching bandwidth of 7 GHz (from 57 to 64) to cover the 60 GHz ISM band. The antenna can be employed in a linear array with around one wavelength distance between the feed points without generating any grating lobes.

The manuscript is organized as follows: in Section II the concept of utilizing diffracted fields is illustrated and generalized. Section III discusses the full-wave simulation results. Section IV discusses the linear antenna array configuration and demonstrates how an array with one wavelength separation between the antenna array elements can be used without generating grating lobes. Section V discusses one of the possible realizations at 60 GHz. Section VI presents a two-element linear antenna array design. Section VII presents the experimental prototyping results. Section VIII concludes and discusses the potential future work.

II. DIPOLE ANTENNA IN-BETWEEN TWO METALLIC SHEETS "INSPIRED BY THE DIFFRACTED FIELDS"

Fig. 1(a) shows a dipole antenna surrounded by two planar metal sheets. The metal sheets can be considered as a special case of a wedge with an exterior wedge angle ($n\pi$) equal to 2π (i.e., n = 2). Fig. 1(b) illustrates the structure as an electric radiating current element in the middle of two diffracting edges (TE case). As the dipole radiating fields
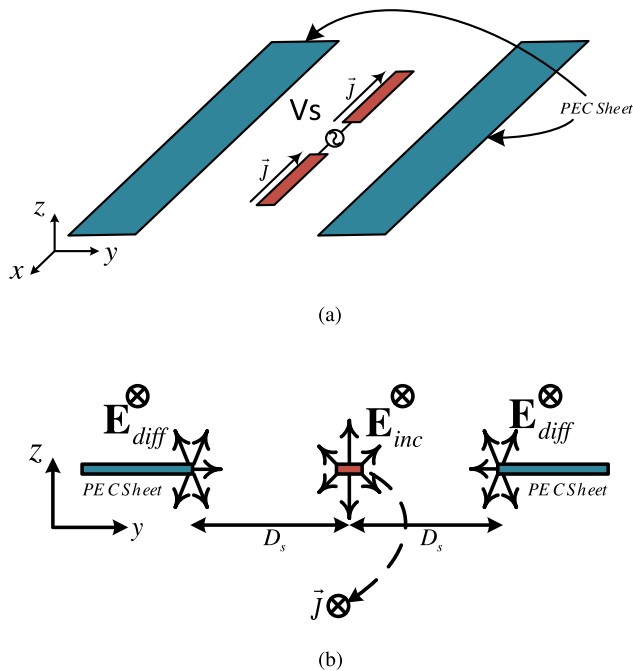
FIGURE 1. Dipole antenna between two metal sheets, (a) 3D geometry, and (b) cross-section indicating the diffracted fields.

impinge on the metal sheets edges, the diffracted fields can be modeled as diffraction sources using the uniform theory of diffraction. The wedge problem has been studied intensively in the literature and has been analyzed mathematically by several techniques. Closed form solution can be obtained using eigenfunction series expansions [8]. Full wave numerical methods, such as the method of moments, are capable of providing an accurate solution as well [9], [10]. Uniform theory of diffraction (UTD) is a powerful method that can be used to analyze the wedge problem. UTD is a ray-based method; it treats scattering problems with intuitive ray model for wave propagation. The ray model is very advantageous as it provides physical insight and allows for better visualization of the field interactions in scattering problems. On the other hand, the uniform theory of diffraction requires that the scattering objects to be electrically large, in the order of a wavelength. Also, as line sources radiate cylindrical waves that can be described by Hankel functions, UTD replaces the Hankel function with its asymptotic approximation as given by (1). For such approximation, the Hankel function argument should be much greater than 1, and hence ($\rho \gg \lambda/2\pi$), where ρ is the distance from the line source. Therefore, the scattering object should be far enough from the line source, and to be electrically large. Therefore, UTD method is usually referred to as a "high-frequency method" [5].

$$H_0^{(2)}(k\rho) \sim \sqrt{\frac{j2}{\pi k}} \frac{e^{-jk\rho}}{\sqrt{\rho}} \qquad (1)$$

We only considered the diffracted fields from the edges close to the electric current source. The metal sheets force

the boundary condition of a zero-tangential electric field, and hence the diffracted fields only appear at the inner edges. From another perspective, those metallic sheets act as soft surfaces for the TE polarized wave produced by the dipole. Therefore, it is expected that there will be no propagation in the y-axis direction, due to the soft surfaces. Also, it is expected that there will be no propagation in the x-axis direction as well, due to the well-known radiation characteristic of the dipole. Consequently, this intuitively implies that most of the radiation will be concentrated along the z-axis, as can be visualized from Fig.1 (b).
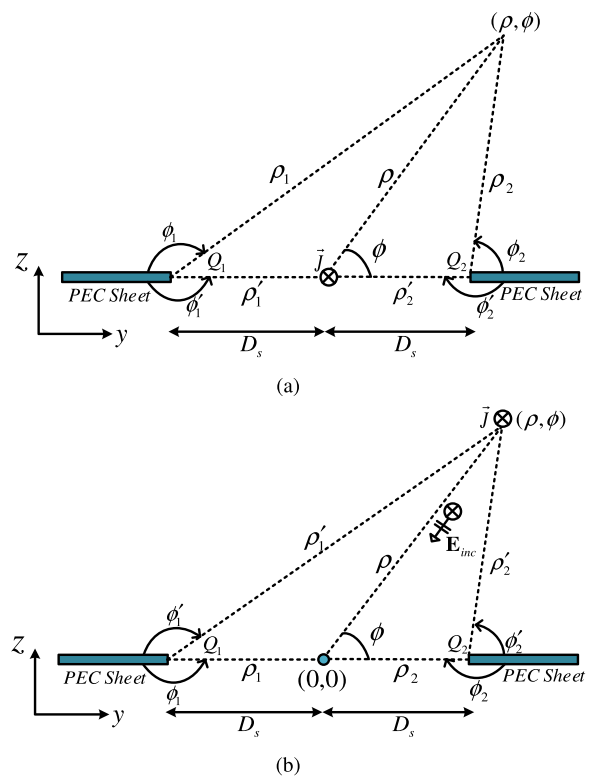

FIGURE 2. UTD analysis of the dipole antenna between two metal sheets, (a) actual problem, and (b) reciprocal problem.

Due to the symmetry along the x-axis, the problem can be solved as a 2D problem. Also, further simplification can be obtained by replacing the dipole by a line source. Moreover, the diffractions at the vertices of the metal sheets are ignored. Despite that, those assumptions and approximations reduce the accuracy of the solution. However, the solution is still suitable to provide all the required physical insights needed for the antenna design. Fig. 2 (a) shows the actual problem and (b) shows the reciprocal version of the same problem.

It is easier to solve the reciprocal version of the problem. In this case, the line source is assumed to be in the far field where it produces an incident plane wave on the metallic sheets. The total field obtained at the origin (the original location of the line source) will be equal to the radiated field at the same angle of incidence in the original problem. By repeating the calculation for all the angles (ϕ), the radiation pattern is obtained. The total field is given by (2). The diffracted field

can be calculated by (3). The diffraction coefficients D_{soi} are calculated using (4) [9], [11] where the subscript 's' refers to the soft case.

$$E_x^{tot} = E_x^{inc} + E_x^{d_1} + E_x^{d_2} \qquad (2)$$

$$E_x^{d_i} = E_x^{inc}(Q_i)D_{soi}\frac{e^{-jk\rho_i}}{\sqrt{\rho_i}} \qquad (3)$$

$$D_{soi} = \frac{-e^{-j\pi/4}}{2n\sqrt{2\pi k}\,\sin(\beta_0)}$$
$$\times \left[\cot\left(\frac{\pi + (\phi_i - \phi_i')}{2n}\right)F(kL_ia^+(\phi_i - \phi_i'))\right.$$
$$+ \cot\left(\frac{\pi - (\phi_i - \phi_i')}{2n}\right)F(kL_ia^-(\phi_i - \phi_i'))$$
$$- \left\{\cot\left(\frac{\pi + (\phi_i + \phi_i')}{2n}\right)F(kL_ia^+(\phi_i + \phi_i'))\right.$$
$$\left.\left. + \cot\left(\frac{\pi - (\phi_i + \phi_i')}{2n}\right)F(kL_ia^-(\phi_i + \phi_i'))\right\}\right] \qquad (4)$$

For the 2D case, $n = 2$, $\beta_0 = \pi/2$, and $\alpha^\pm(\beta) = 2\cos^2(\beta/2)$, and $F(X)$ is the transition function given in (5).

$$F(X) = j2\sqrt{X}e^{jX}\int_{\sqrt{X}}^{\infty}e^{-jt^2}dt \qquad (5)$$

The structure in Fig. 1 can be perceived as three radiating elements (i.e., the dipole and the two diffraction sources). In this case, if the radiation of the three sources adds up constructively in the boresight direction, high gain can be achieved in the boresight. The problem can be further simplified for the boresight direction ($\phi = 90°$). The total electric field in $\phi = 90°$ direction as a function of D_s is given in (6). The derivation details are provided in appendix.

$$E_x^{tot} = E_0\left(1 - F\left(2\pi\frac{D_s}{\lambda}\right)\frac{\sqrt{2\lambda/D_s}}{\pi}e^{-j(kD_s+\pi/4)}\right) \qquad (6)$$

The second term of (6) resembles a Lituus spiral. In this case, the trace of the spiral can be roughly approximated with concentric circles centered at the spiral center. Fig. 3 shows a graphical representation of (6) in the complex plane. Hence, the maximum of (6) can be obtained when the second term phase is an odd integer multiple of π. Hence, the peaks in the gain as a function of the distance from the dipole can be roughly approximated as given in (7). The derivation details are also provided in Appendix.

$$D_{s\,max} = \frac{(4n_o - 1)}{8}\lambda \qquad (7)$$

where, n_o is a non-zero odd integer number ($n_o = 1, 3, 5, ..$).

The above analysis indicates that the gain boost due to the diffraction sources adds to the original dipole gain in the boresight direction, which can be calculated easily. Fig. 4 shows the gain boost in dB versus the distance D_s. The calculated values have been verified by simulated results using FEKO; the solver settings were adjusted to UTD method. A good match between the calculated and FEKO simulated results
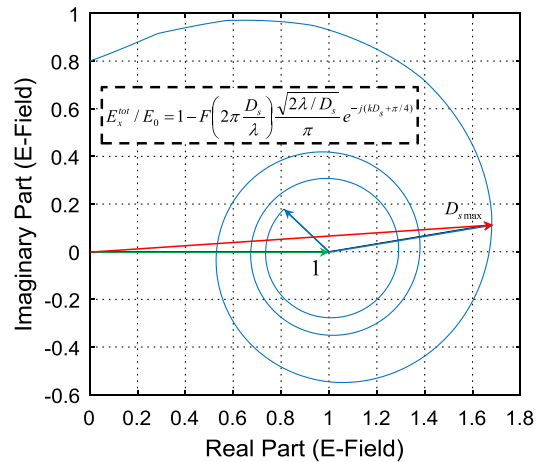
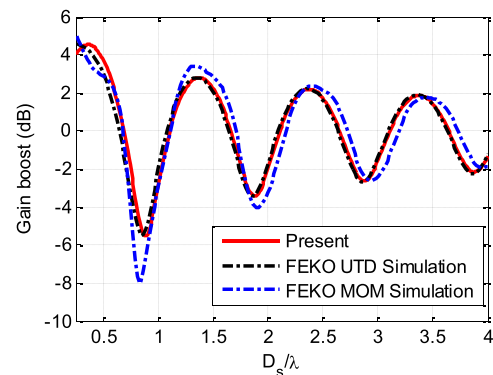**FIGURE 3.** Graphical representation of the complex plane from (6).

FIGURE 4. Gain boost (dB) versus Ds/λ.

is observed as shown in Fig. 4. The oscillatory behavior in Fig. 4 is due to the variation of the phase of the induced diffraction sources. As the metal sheets edge separation from the dipole increase, the phase of the induced diffraction sources varies in a periodic fashion. Also, the diffracted sources intensities get weaker as the sheets move further away from the source. This explains the decaying behavior in Fig. 4. The peaks of the gain occur when the diffraction sources radiation adds up constructively to the dipole radiation, and the dips happen when they add up destructively.

The peak boost in the gain happens when $\{D_s = 0.375\lambda\}$ an increase of 4.54 dB is obtained. On the other hand, the gain boost that can be obtained by having three element array is $\{10\log_{10}(3) = 4.77\ dB\}$. Therefore, it seems that the structure is acting as a three-element array (i.e., dipole and two diffracted sources).

To focus the radiation in one direction a PEC reflector sheet can be used below the radiating structure as shown in Fig. 5. This concept can be further generalized for the dual problem where the dipole can be replaced by a magnetic current source (such as a slot antenna). Then, the PEC sheets can be replaced by PMC sheets. As there is no real physical magnetic conductor, periodic structures or high dielectric constant material
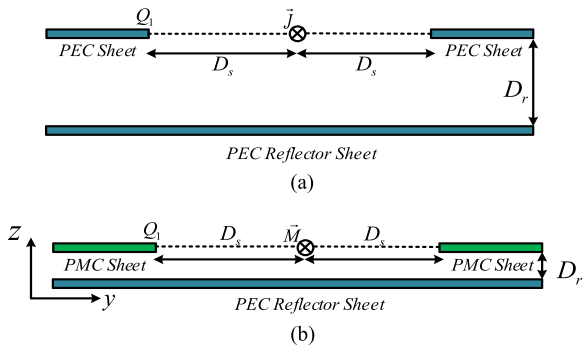
FIGURE 5. Dual electric and magnetic problems. (a) Electric current problem. (b) Magnetic current problem.

can realize artificial magnetic conductor. In the electric case the reflector distance from the antenna should be a quarter wavelength, and for the magnetic case, it can be placed very close to the antenna [12].
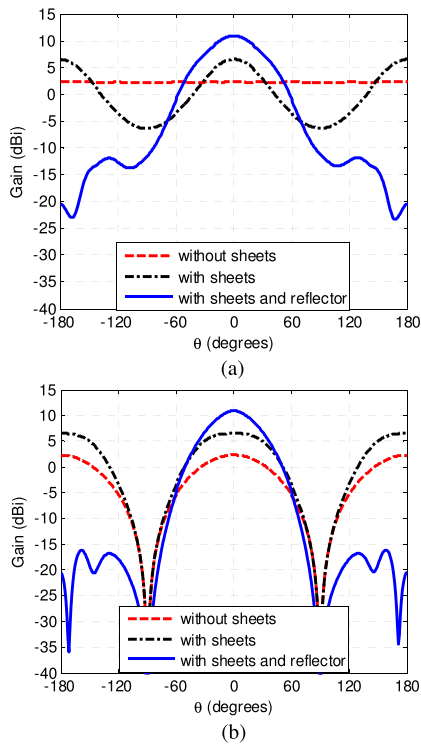

FIGURE 6. Radiation patterns in principle planes, (a) H-Plane, and (b) E-Plane.

III. FULL WAVE ANALYSIS

Fig. 6 shows the full wave analysis radiation patterns in the principal planes. In the simulation, the width of the sheet used is a quarter wavelength, and the distance D_s is 0.375λ. The structure is backed by a PEC reflector as proposed in Fig. 5 with $D_r = 0.25\lambda$. As it can be noticed from Fig. 6, with a single dipole a gain of around 11.5 dBi is obtained, and all the radiation is focused in the boresight direction.

We should emphasize that UTD ray optical field analysis is accurate as long as the observation point is far enough from the transition region and the edge [9], [13]. Therefore, it is noticed in Fig. 4 that the smallest D_s value is 0.2λ. Also, as previously stated, the diffraction from the sheet vertices is ignored, and the dipole antenna is approximated with a line source. With all those assumptions and approximations, it is expected that UTD solution to be less accurate once compared with the full wave solution (such as the method of moment solution). Fig. 4 shows some deviation for the method of moment solution over UTD solution as we ignored the slope diffraction from the second edge (far edge) and the multiple diffractions of the metal plate between the edges. However, from an antenna designer perspective, the UTD solution is compelling in providing physical insight into the antenna design. For example, even by knowing that the PEC acts as a soft surface for the TE polarization of the dipole, it is still not clear what would be the proper distance of the sheets to achieve maximum boresight gain. Also, UTD intuitive model provides excellent interpretation of the physical interaction of the fields in the problem through the definition of diffraction sources. Such interpretation is a bit hard to grasp in other numerical methods. Therefore, with such basic UTD analysis, and with the aid of full wave solver, high gain antennas can be designed and optimized easily.
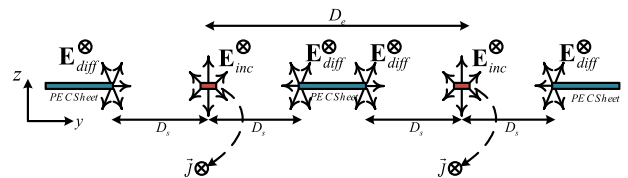

FIGURE 7. Two elements array configuration.

IV. LINEAR ANTENNA ARRAY

It was shown from previous analysis that the distance from the dipole to the metal sheet near the edge is 0.375λ, and the sheet width is 0.25λ. Therefore, the width of the antenna is 1.25λ. The question that would arise is it possible to employ this antenna in a linear antenna array without generating grating lobes? The answer is simply, yes. Fig. 7 shows the configuration of a two-element antenna array. As can be noticed, the middle sheet is shared between the two elements on the right and left sides. In this case, the diffraction sources, and the real sources (i.e., dipoles) are almost in phase, and all their radiation adds up constructively. Thus, the distance between the radiating elements is less than a half wavelength, where the radiating elements are not only the real sources (i.e., the dipoles) but also include the induced diffraction sources at the edges of the sheet. From another perspective, the two elements are considered overlapping by sharing the quarter wavelength sheet in between.

According to the previous discussion, a tremendous advantage is obtained, where the distance between the elements to be fed can exceed a half wavelength to a one-wavelength.
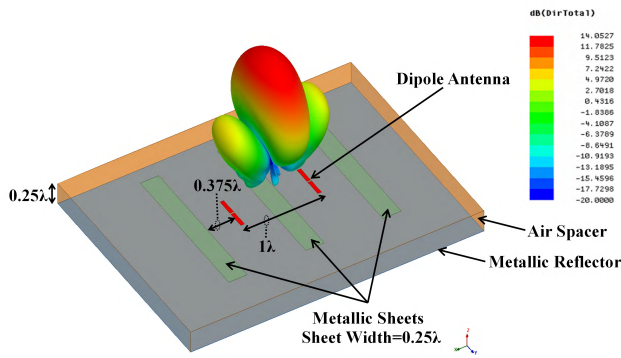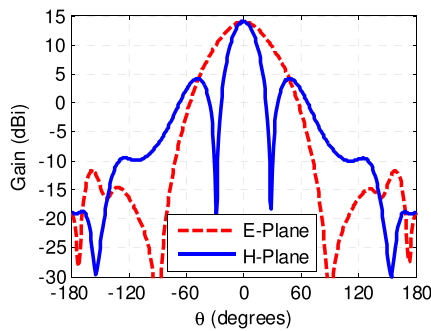
FIGURE 8. Full wave simulation.

FIGURE 9. Radiation pattern in principle planes.

FIGURE 10. Proposed antenna structure, (a) 3D view, (b) top view, and (c) bottom view.

TABLE 1. Antenna structure dimensions.

Dimension	A	B	C	D	E	F	G
Value (mm)	1.5	0.71	1.55	0.31	1.9	6	2

FIGURE 11. S_{11} and gain values for the proposed antenna structure.

Eventually, this provides higher flexibility in the design of the feeding networks, especially at high frequencies. Fig. 8 shows the full wave simulation for two dipoles separated by 1λ (sheet width is 0.25λ, and D_s is 0.375λ). Fig. 9 shows the radiation patterns in the principal planes of the same structure. It is noticed that there are no grating lobes. Another advantage is that by having the PEC sheets between the fed dipoles (acting as soft surfaces) [14], a very low mutual coupling is obtained between the array elements.

V. REALIZATION AT MILLIMETER-WAVE FREQUENCIES

The proposed antenna configuration acts as an excellent candidate to realize high gain antennas at millimeter-wave frequencies. In this case, a planar monopole fed with microstrip-line is used to realize a high gain antenna at 60 GHz. Fig. 10 shows the proposed antenna structure. Table 1 lists the corresponding dimensions of the proposed structure. Rogers RO-3003 substrate with a dielectric constant of 3 is used. The thickness of the substrate is 0.13 mm. An air spacer of 1.1 mm separates the antenna from a plane metallic reflector. The structure is low profile, fully planar, and requires no vias. The simplicity of the structure makes it less susceptible to manufacturing tolerances. Also, it makes it very attractive as a low-cost structure.

Fig. 11 shows the corresponding S_{11} and gain values. The antenna is matched over the whole range of the 60 GHz ISM band (i.e., from 57 to 64 GHz). The boresight gain is 11 dBi with very good stability over the matching bandwidth.
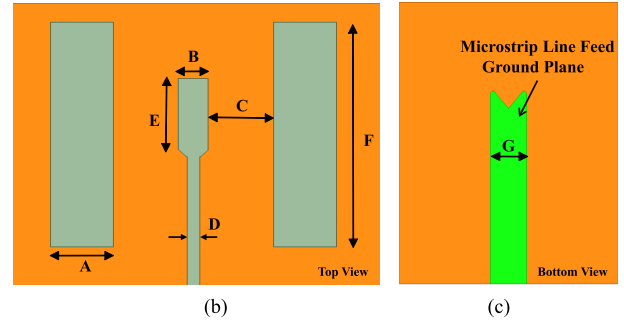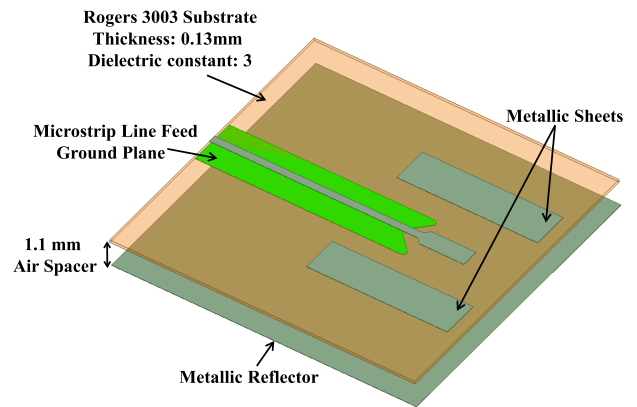
Fig. 12 shows the radiation patterns in the principal planes. A slight tilt is observed in the beam (i.e., in E-Plane) due to the asymmetry of the nature of the printed planar monopole fed by microstrip line instead of a center fed dipole. Also, from Fig. 11, the tilt effect can be noticed as the difference between the maximum gain and the boresight gain, which is around 0.5 dB. The radiation pattern is stable over the frequency band with low cross-polarization levels. This makes the antenna, a very suitable low-cost, low profile, and high gain solution for short range high data rate wireless applications at 60 GHz.
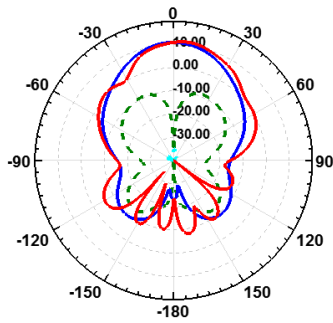
FIGURE 12. Principal planes radiation patterns of the antenna structure at 60 GHz, (solid lines refer to a co-polar component (H-Plane: Blue, and E-Plane: Red), and dashed lines refer to a cross-polar component (H-Plane: Green, and E-Plane: Cyan)).
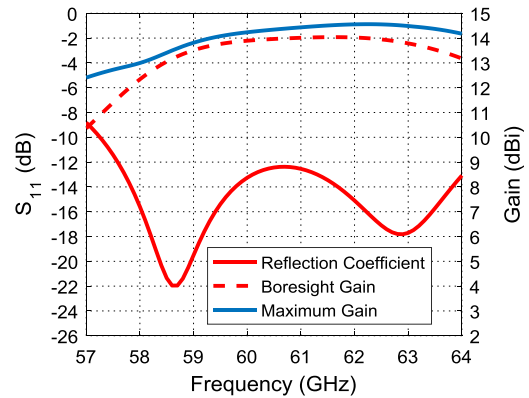

(a)

(b)   (c)

FIGURE 13. Proposed two-element antenna array structure, (a) 3D view, (b) top view, and (c) bottom view.

FIGURE 14. S_{11} and gain values for the proposed two-element antenna array structure.

FIGURE 15. Mutual coupling between the adjacent elements in the two-element array.

FIGURE 16. Principal planes for the two-element array at 60 GHz, (solid lines refer to a co-polar component (H-Plane: Blue, and E-Plane: Red), and dashed lines refer to a cross-polar component (H-Plane: Green, and E-Plane: Orange)).

VI. TWO-ELEMENT ARRAY

The proposed antenna design has been employed for a two-element array. Fig. 13 shows the two-element array structure. Fig. 14 shows the corresponding matching and gain values.

As expected, an extra 3 dBi of gain is achieved (i.e., a gain of 14 dBi from the two-element array). The distance between the feeding lines is 5.3 mm, which is 1.06λ. Fig. 16 shows the radiation patterns with no grating lobes. This feature makes such solution very desirable where it provides great flexibility in the design of the feeding networks, which is considered to be a major challenge at millimeter-wave
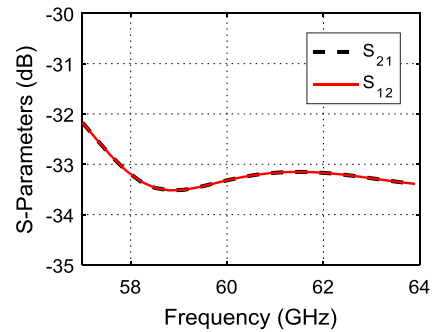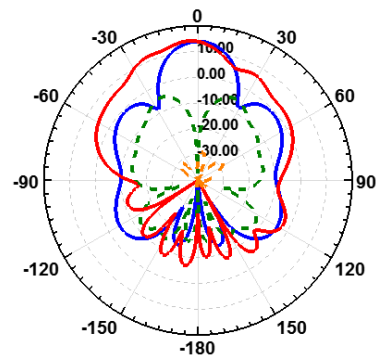
frequencies. In such a case the distance between the feed lines is almost one free space wavelength rather than being half free space wavelength. Also, as the metallic sheets act as soft surfaces, the mutual coupling between the antenna elements is reduced significantly. Fig. 15 shows that the coupling between the adjacent elements is less than −30 dB over the whole bandwidth.

VII. EXPERIMENTAL PROTOTYPING RESULTS

The proposed structures are fabricated and tested in an anechoic chamber. Fig. 17 shows the photos of the single
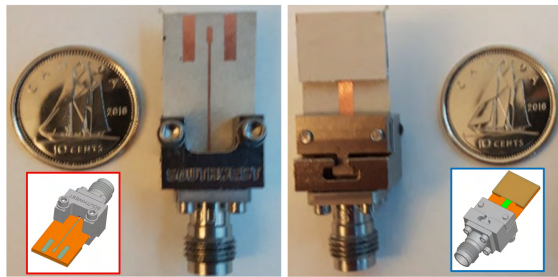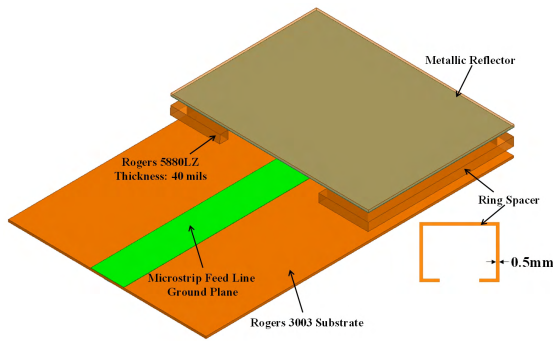
FIGURE 17. Proposed single element antenna spacer and actual prototype model.

FIGURE 18. Single element realized gain and reflection coefficient.

FIGURE 19. Single element radiation patterns in principal planes (solid lines refers to simulated data, and dashed lines refers to measured data) E-Plane (left) and H-plane (right) 57, 60 and 63 GHz from top to bottom.

FIGURE 20. Two-element antenna array actual prototype model.

element. To realize the reflector, a ring is made of a Rogers-5880LZ substrate as demonstrated in Fig. 17 to provide the spacer needed. The choice of Rogers 5880LZ is attributed to its low permittivity ($\varepsilon_r = 2$), the permittivity of the ring is desired to be as low as possible to prevent the excitation of any possible modes in the cavity like region below the antenna (i.e., ring material is desired to be as close to free space as possible). Other ways to realize the spacer is using a dielectric substrate. However, the use of dielectric substrate causes some additional losses in the form of surface waves in the substrate, and hence reduces the gain. Although an AMC reflector can be located in close proximity to the antenna and maintains lower quality factor (i.e., wider bandwidth), the PEC reflector is used that requires a quarter wavelength distance from the antenna that increases the quality factor (i.e., lower bandwidth) as explained thoroughly in [15]. This is justified by the fact that the dimensions of the AMC structure unit cell should be much smaller than the operating wavelength [16], and as the free space quarter wavelength at 60 GHz is 1.25 mm, the design of such unit cell will have very small dimensions that requires much higher precision to fabricate, and will be more susceptible to fabrication tolerances. Also, from the gain point of view, the PEC reflector has better performance in terms of gain, once compared with AMC reflectors [15]. From an application perspective, the gain should not be compromised. Moreover, the monopole/PEC-reflector structure matching bandwidth is still wide enough to cover the 60 GHz ISM band.

Fig. 18 shows the measured and simulated results of both the realized gain and reflection coefficient. A good agreement between measured and simulated results is observed. Fig. 19 shows the simulated and measured normalized
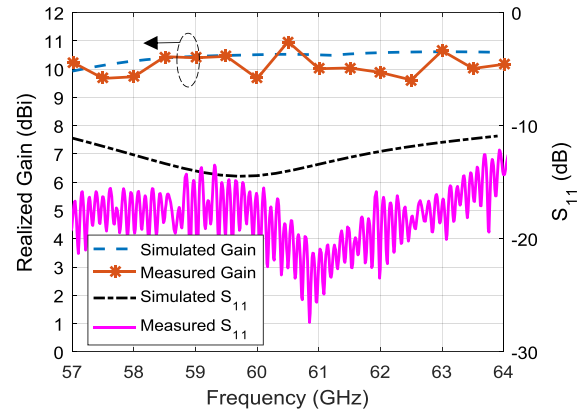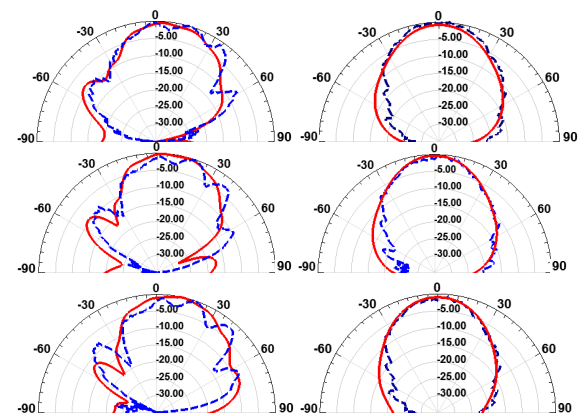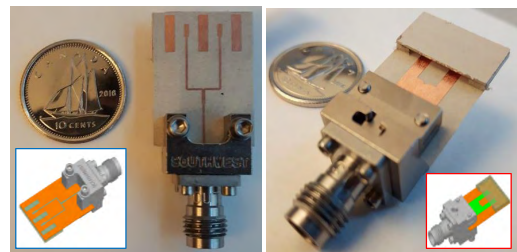
radiation patterns in the principal planes. An acceptable agreement is observed as well.

Fig. 20 shows the two-element array structure prototype. Fig. 21 shows the measured and simulated results of both the realized gain and reflection coefficient. A good agreement between measured and simulated values is observed. Fig. 22 shows the simulated and measured normalized radiation patterns in the principal planes. An acceptable agreement is observed as well.

It was noticed that the reflector ring is a key source of tolerance errors. The substrate thickness is 0.13 mm, which leaves around 1.12 mm distance from the antenna to the PEC

FIGURE 21. Two-element array realized gain and reflection coefficient.

FIGURE 22. Two-element array radiation patterns in principal planes (solid lines refers to simulated data, and dashed lines refers to measured data) E-Plane (left) and H-plane (right) 57, 60 and 63 GHz from top to bottom.
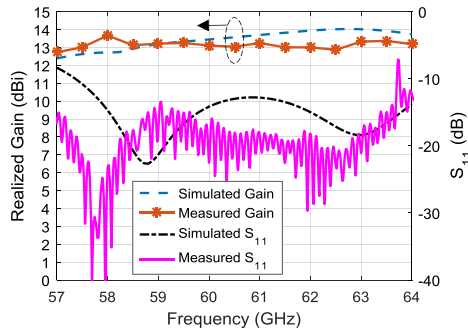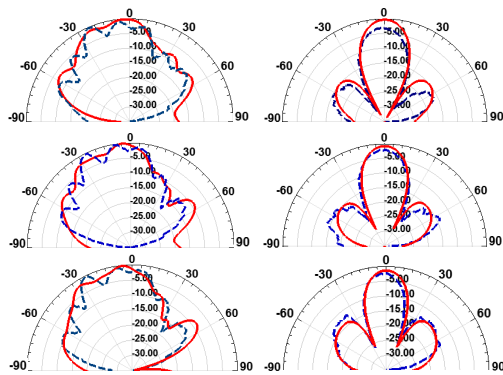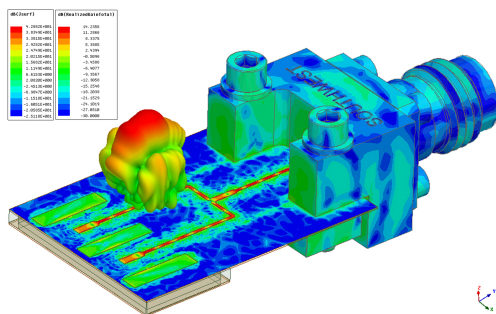

FIGURE 23. Surface current density heat map and 3D radiation pattern of the two-element antenna array.
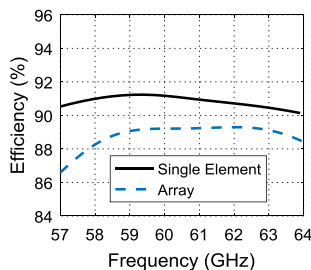

FIGURE 24. Calculated efficiency of the single element and two element array structures.

reflector, such physical dimension of the ring is a point to consider in terms of the mechanical stability, especially, when attached to a very thin and fragile 0.13 mm substrate. The

size of the connector is considerably large, and its existence in the vicinity of the antenna environment can be thought of as a large scatterer. To reduce its effect, the feeding line is extended to have the antenna as far as possible from the connector body. The expense of increasing the feed line length is a higher level of dielectric losses as expected.

Fig. 24 shows the induced surface currents from the antenna on the connector body. Also, as the feed line width is very small (0.3 mm), the connector pin alignment of the connector at the center of the line is very critical, in order to have proper excitation of the antenna. Therefore, it is suggested that characterizing the antenna using a probing station can facilitate a more seamless and accurate characterization for such an antenna. It is worth noting that the connector with long feeding line exists only for measurement and characterization purposes. However, in the practical integrated system, the antenna is incorporated directly next to the circuitry stages, which could usually be a bandpass filter or an amplifier. Thus, such deterioration can be mitigated. In the measured radiation patterns, we can see the ripples in the main beam. These ripples are due to the interaction of the antenna with the mounting structure. As seen in Fig. 23, the strong current on the connector makes it interact with the surrounding that is not considered in the simulation.

Fig. 24 shows the calculated efficiency of both the single element and array, as expected the array structure is less efficient due to the higher losses in the feeding structure.

VIII. CONCLUSION AND FUTURE WORK

Diffracted fields from planar metal sheets have been utilized to implement high gain, low profile, and low-cost antenna at 60 GHz. The proposed antenna has been matched over the 60 GHz ISM band (57 – 64 GHz). The antenna gain is 11 dBi. The proposed antenna has been employed in a linear array with one wavelength distance between array elements without generating grating lobes. The proposed structure suits short range, low power applications, such as wireless personal area networks (WPAN). The proposed structure avoids using vias and any complex fabrication requirements, in such a way that it can be realized in any modest fabrication facility. Suggested future work can include various realizations of the proposed concept. One other possible realization is the use of a slot antenna instead of the dipole, and the use of high dielectric constant thick sheets such as silicon instead of the metal sheets. Future work also can include the study of different feeding mechanisms that would eliminate the tilt in the E-plane radiation pattern, such as using shielded feeding network, and dual feed of the element. In addition, the study of employing such element in a large scale array.

APPENDIX
DERIVATION OF THE TOTAL ELECTRIC FIELD USING UTD

The parameters for the reciprocal problem shown in Fig.2 are given as follows:

$$\phi_1 = \phi_2 = \pi, \phi_1' = \phi, \phi_2' = \pi - \phi, L_i = \rho_i, \rho_1 = \rho_2 = D_s$$

The incident electric field at the edges can be written as:

$$E_x^{inc}(Q_1) = E_0 e^{jk\rho_1 \cos(\phi)} \tag{8}$$

$$E_x^{inc}(Q_2) = E_0 e^{-jk\rho_2 \cos(\phi)} \tag{9}$$

For boresight ($\phi = 90°$), the derivation of (6) can be obtained as follows:

$$D_{so1} = D_{so2} = D_{so} \tag{10}$$

$$E_x^{inc}(Q_1) = E_x^{inc}(Q_2) = E_0 \tag{11}$$

$$E_x^{inc}(0,0) = E_0 \tag{12}$$

$$E_x^{d_i} = E_0 D_{so} \frac{e^{-jkD_s}}{\sqrt{D_s}} \tag{13}$$

$$D_{so} = \frac{-e^{-j\pi/4}\sqrt{\lambda}}{8\pi} F(kD_s) \left(\begin{array}{c} \cot\left(\frac{3\pi}{8}\right) + \cot\left(\frac{\pi}{8}\right) \\ -\cot\left(\frac{5\pi}{8}\right) - \cot\left(\frac{-\pi}{8}\right) \end{array} \right) \tag{14}$$

$$D_{so} = \frac{-e^{-j\pi/4}\sqrt{\lambda/2}}{\pi} F\left(2\pi \frac{D_s}{\lambda}\right) \tag{15}$$

$$E_x^{tot} = E_x^{inc} + E_x^{d_1} + E_x^{d_2} \tag{16}$$

$$E_x^{tot} = E_0 + 2E_0 D_{so} \frac{e^{-jkD_s}}{\sqrt{D_s}} = E_0\left(1 + 2D_{so}\frac{e^{-jkD_s}}{\sqrt{D_s}}\right) \tag{17}$$

This concludes that the total electric field in the boresight direction as a function of D_s can be written as given by (18).

$$E_x^{tot} = E_0 \left(1 - F\left(2\pi \frac{D_s}{\lambda}\right) \frac{\sqrt{2\lambda/D_s}}{\pi} e^{-j(kD_s + \pi/4)}\right) \tag{18}$$

The second term of (6) resembles a Lituus spiral. In this case, the trace of the spiral can be roughly approximated with concentric circles centered at the spiral center. Hence, the approximate maximum of (6) can be obtained when the second term phase is an odd integer multiple of π, and the approximate minimum when it is even multiple integers of π. Hence, the peaks and the dips in the gain as a function of the distance from the dipole can be written as follows:

For the peaks $\rightarrow kD_s + \pi/4 = n_o\pi$

Where n_o is a non-zero odd integer number ($n_o = 1, 3, 5, ..$)

$$D_s = \frac{(4n_o - 1)}{8}\lambda \rightarrow D_{s\,max} = 0.375\lambda, 1.375\lambda, 2.375\lambda, \ldots$$

For the dips $\rightarrow kD_s + \pi/4 = n_e\pi$

Where n_e is a non-zero even integer number ($n_e = 2, 4, 6, ..$)

$$D_s = \frac{(4n_e - 1)}{8}\lambda \rightarrow D_{s\,min} = 0.875\lambda, 1.875\lambda, 2.875\lambda, \ldots$$

REFERENCES

[1] F. A. Wyczalek, *Millimeter Wave Technology in Wireless PAN, LAN, and MAN*. Boca Raton, FL, USA: CRC Press, 2008.

[2] D. Liu, B. Gaucher, U. Pfeiffer, and J. Grzyb, *Advanced Millimeter-Wave Technologies*. Chichester, U.K.: Wiley, 2009.

[3] C. Kärnfelt, P. Hallbjörner, H. Zirath, and A. Alping, "High gain active microstrip antenna for 60-GHz WLAN/WPAN applications," *IEEE Trans. Microw. Theory Techn.*, vol. 54, no. 6, pp. 2593–2602, Jun. 2006.

[4] X.-P. Chen, K. Wu, L. Han, and F. He, "Low-cost high gain planar antenna array for 60-GHz band applications," *IEEE Trans. Antennas Propag.*, vol. 58, no. 6, pp. 2126–2129, Jun. 2010.

[5] Y. J. Cheng, *Substrate Integrated Antennas and Arrays*, 1st Ed. Boca Raton, MA, USA: CRC Press, 2015.

[6] K.-S. Chin, W. Jiang, W. Che, C.-C. Chang, and H. Jin, "Wideband LTCC 60-GHz antenna array with a dual-resonant slot and patch structure," *IEEE Trans. Antennas Propag.*, vol. 62, no. 1, pp. 174–182, Jan. 2014.

[7] A. A. Qureshi, D. M. Klymyshyn, M. Tayfeh, W. Mazhar, M. Borner, and J. Mohr, "Template-based dielectric resonator antenna arrays for millimeter-wave applications," *IEEE Trans. Antennas Propag.*, vol. 65, no. 9, pp. 4576–4584, Sep. 2017.

[8] C. A. Balanis, *Advanced Engineering Electromagnetics*, 2nd ed. Hoboken, NJ, USA: Wiley, 2012.

[9] R. Paknys, *Applied Frequency-Domain Electromagnetics*. Chichester, U.K.: Wiley, 2016.

[10] Y. T. Lo and S. W. Lee, Eds., *Antenna Handbook*. Boston, MA, USA: Springer, 1988.

[11] R. G. Kouyoumjian and P. H. Pathak, "A uniform geometrical theory of diffraction for an edge in a perfectly conducting surface," *Proc. IEEE*, vol. 62, no. 11, pp. 1448–1461, Nov. 1974.

[12] C. A. Balanis, Ed., *Modern Antenna Handbook*, 1st ed. Hoboken, NJ, USA: Wiley, 2008.

[13] L. B. Felsen, "Evanescent waves," *J. Opt. Soc. Amer.*, vol. 66, no. 8, pp. 751–760, 1976.

[14] P. S. Kildal, A. A. Kishk, and S. Maci, "Special issue on artificial magnetic conductors, soft/hard surfaces, and other complex surfaces," *IEEE Trans. Antennas Propag.*, vol. 53, no. 1, pp. 2–7, Jan. 2005.

[15] A. Vallecchi, J. R. De Luis, F. Capolino, and F. De Flaviis, "Low profile fully planar folded dipole antenna on a high impedance surface," *IEEE Trans. Antennas Propag.*, vol. 60, no. 1, pp. 51–62, Jan. 2012.

[16] H. Nakano, *Low-Profile Natural and Metamaterial Antennas*. Hoboken, NJ, USA: Wiley, 2016.

YAZAN AL-ALEM received the B.Sc. degree in electrical engineering from The University of Jordan in 2010 and the M.Sc. degree in electrical engineering from the American University of Sharjah in 2015. He is currently pursuing the Ph.D. degree with Concordia University, Montréal, QC, Canada. He received the Concordia University International Tuition Award of Excellence, and the American University of Sharjah Full Graduate Teaching and Research Assistantship.

AHMED A. KISHK received the B.S. degree in electronic and communication engineering from Cairo University, Cairo, Egypt, in 1977, the B.Sc. degree in applied mathematics from Ain-Shams University, Cairo, Egypt, in 1980, and the M.Eng. and Ph.D. degrees from the Department of Electrical Engineering, University of Manitoba, Winnipeg, Canada, in 1983 and 1986, respectively. In 1986, he joined the Department of Electrical Engineering, University of Mississippi. He was a Professor with the University of Mississippi from 1995 to 2011. He has been a Professor with Concordia University, Montréal, QC, Canada, since 2011. He is currently the Tier 1 Canada Research Chair in advanced antenna systems. He was the 2017 AP-S President.

He has published over 320-refereed journal articles and 450 conference papers. He has co-authored four books and several book chapters. His research interests include the areas of millimeter wave antennas for 5G applications, Analog beamforming network, antennas, microwave passive circuits and components, EBG, artificial magnetic conductors, phased array antennas, reflect/transmitarray, and wearable antennas. He is an editor of three books.

• • •